iScience

CellPress
OPEN ACCESS

Article

Hedgehog signaling is required for endometrial remodeling and myometrial homeostasis in the cycling mouse uterus

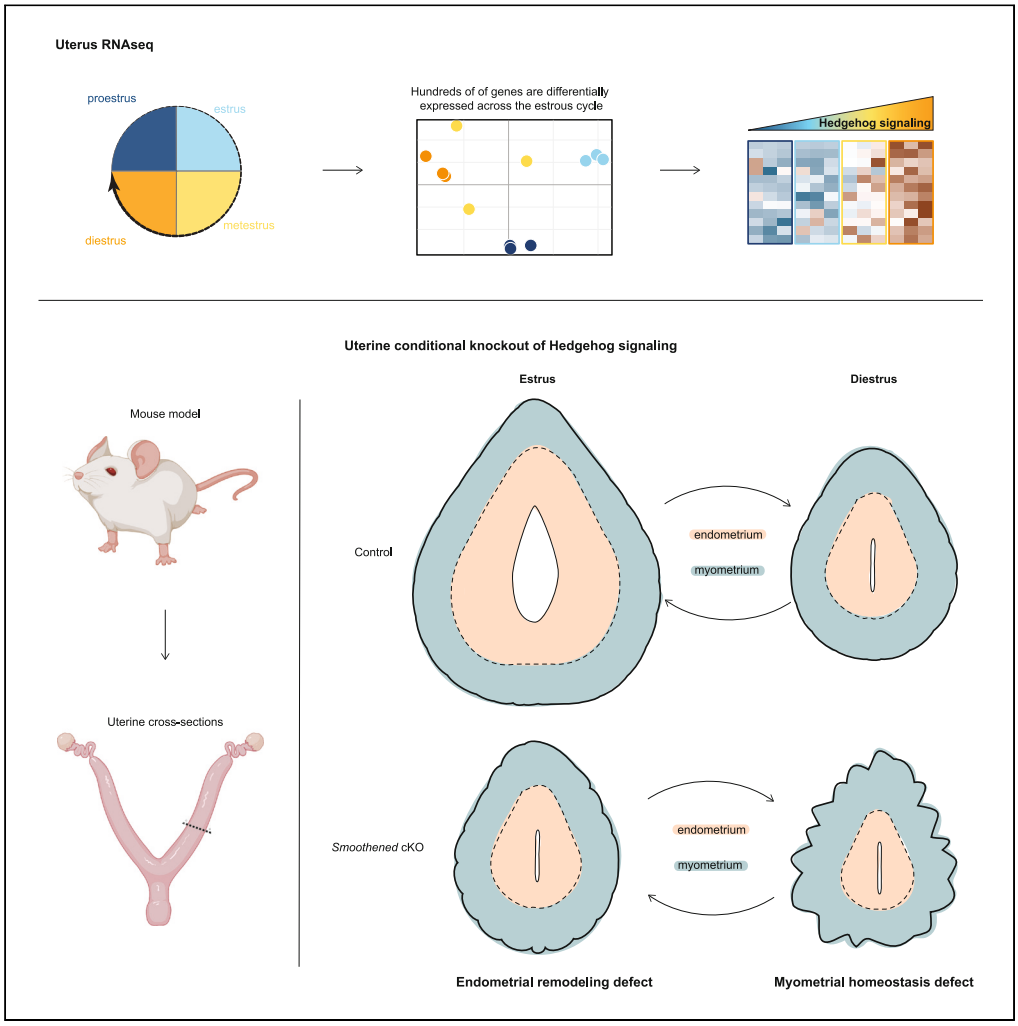

Elle C. Roberson, Ngan Kim Tran, Anushka N. Godambe, ..., LeCaine J. Barker, Rebecca D. Fitch, John B. Wallingford

elle.roberson@cuanschutz.edu (E.C.R.)
wallingford@austin.utexas.edu (J.B.W.)

Highlights

Hedgehog signaling components are similarly enriched across the estrous cycle

Smoothened is required for uterine endometrial remodeling

Smoothened is required for uterine myometrial homeostasis

Roberson et al., iScience 26, 107993
October 20, 2023
https://doi.org/10.1016/j.isci.2023.107993

iScience

CellPress
OPEN ACCESS

Article

Hedgehog signaling is required for endometrial remodeling and myometrial homeostasis in the cycling mouse uterus

Elle C. Roberson,[1,3,*] Ngan Kim Tran,[2] Anushka N. Godambe,[2] Harrison Mark,[2] Michelle Nguimtsop,[2] Trinity Rust,[2] Elizabeth Ung,[1] LeCaine J. Barker,[1] Rebecca D. Fitch,[2] and John B. Wallingford[2,*]

SUMMARY

Decades of work demonstrate that the mammalian estrous cycle is controlled by cycling steroid hormones. However, the signaling mechanisms that act downstream, linking hormonal action to the physical remodeling of the cycling uterus, remain unclear. To address this issue, we analyzed gene expression at all stages of the mouse estrous cycle. Strikingly, we found that several genetic programs well-known to control tissue morphogenesis in developing embryos displayed cyclical patterns of expression. We find that most of the genetic architectures of Hedgehog signaling (ligands, receptors, effectors, and transcription factors) are transcribed cyclically in the uterus, and that conditional disruption of the Hedgehog receptor *smoothened* not only elicits a failure of normal cyclical thickening of the endometrial lining but also induces aberrant deformation of the uterine smooth muscle. Together, our data shed light on the mechanisms underlying normal uterine remodeling specifically and cyclical gene expression generally.

INTRODUCTION

Repeated cycles of gene expression are central to diverse aspects of biology, from the Period and Cryptochrome (PER/CYC)-mediated cycles that drive circadian rhythm[1] to the Notch-mediated clock and wavefront that generates the blocks of embryonic somites.[2] It is interesting then that while decades of research have defined the crucial roles of steroid hormone cycles in control of the mammalian estrous cycle,[3,4] far less is known of the cyclical patterns of gene expression that link those hormones to cyclical changes in the structure of the reproductive tract.

Indeed, the uterus is unlike other adult tissues as it repeatedly undergoes extensive remodeling during the estrous cycle, implantation, and pregnancy. In some mammals, such as humans, the uterine lining is cyclically shed in the process of menstruation. However, most mammals do not menstruate and instead undergo a reiterative process of tissue remodeling across the estrous cycle. In the mouse, the endometrial lining of the uterus thickens and elaborates when estrogen increases during the first half of the estrous cycle, and this lining dramatically thins and simplifies in the second half, when progesterone increases.[3,4] Over this time frame, new studies have shown that luminal epithelium turns over[5] and the ratio between stromal and epithelial cells shifts dramatically.[6] However, the gene regulatory mechanisms that act downstream of cycling hormone signals to drive the tissue behaviors underlying cyclical uterine remodeling are not known.

For example, endometrial *Indian hedgehog* (*Ihh*) is a direct target of progesterone and drives remodeling during pregnancy and implantation in the rodent,[7–10] and others have shown that *Ihh* is cyclically controlled during the menstrual[11] and estrous cycle.[12,13] But the function of Hedgehog signaling in the non-pregnant, cycling uterus is unknown, and previous bulk RNA sequencing (RNA-seq) studies[12,13] have focused on only two stages. Moreover, while these genomic datasets of the cycling endometrium in humans[14–18] and rodents[6] have begun to illuminate the transcriptome of the non-pregnant uterus, our knowledge of how downstream signaling pathways contribute to cyclical remodeling and homeostasis is sparse. Given the power of mouse genetics to explore mammalian biology, this gap in knowledge presents a key hurdle.

Here, we fill that gap by determining the transcriptomic landscape of the cycling adult mouse uterus at every stage of the estrous cycle. Interestingly, these data suggest that uterine remodeling requires robust re-use of genetic systems more commonly associated with embryonic development, including Hox family transcription factors and Wnt, transforming growth factor β (TGF-β), and Hedgehog signaling. For the latter case, we show that the majority of the signaling pathway undergoes robust cyclical transcription and that loss of Hh signaling not only severely perturbs normal cyclical remodeling of the uterus but also induces an aberrant remodeling of the smooth muscle tissue in the myometrium. Our work on the normal estrous cycle may shed light on other aspects of myometrial biology, like pregnancy and parturition, or the progression of uterine smooth muscle tumors.

[1]Department of Pediatrics, Section of Developmental Biology, University of Colorado Anschutz Medical School, Aurora, CO 80045, USA
[2]Department of Molecular Biosciences, University of Texas at Austin, Austin, TX 78712, USA
[3]Lead contact
*Correspondence: elle.roberson@cuanschutz.edu (E.C.R.), wallingford@austin.utexas.edu (J.B.W.)
https://doi.org/10.1016/j.isci.2023.107993

RESULTS

Quantification of uterine remodeling across the mouse estrous cycle

We sought to understand the molecular/genetic changes that accompany the iterative remodeling of the normal mouse uterus, so we first extended previous studies[3,4] by developing a comprehensive set of morphometrics to quantify normal uterine morphology across the estrous cycle. We therefore visualized gross tissue morphology of uteri at each estrous cycle stage using H&E staining (Figures 1A–1D, n = 8 per stage) and independently quantified diverse uterine compartments.

The total uterus area was thickest at proestrus and then steadily decreased until diestrus (Figure 1E), and the area of the lumen followed a similar pattern (Figure 1F). The endometrium was also thickest at proestrus and thinnest at diestrus (Figure 1G). We also quantified the number of uterine glands and the luminal epithelial cell height in the endometrium across the estrous cycle; both were highest at proestrus and lowest at diestrus (Figures 1I and 1J). By contrast, while the myometrium displays cyclical spontaneous contractile activity during the estrous cycle,[19] overall myometrial area was not significantly altered across the estrous cycle (Figure 1H). Thus, the normal cycling endometrium displays several cyclical changes in gross morphology across the estrous cycle while the myometrium does not.

The murine uterus is transcriptionally dynamic across the estrous cycle

We hypothesized that downstream of steroid hormones, a variety of signaling pathways might be utilized in the adult uterus to regulate cyclical tissue remodeling. To test this hypothesis, we performed 3′ TagSeq of the whole uterus at each stage of the estrous cycle (n = 3 per stage). Principal-component analysis (PCA) of three biological replicates per estrous cycle stage showed clear separation of estrous cycle replicates, with PC1 and PC2 accounting for 49% and 22% of the variance, respectively (Figure 1K). While most samples within each stage cluster well together, we noted that the metestrus samples (in yellow) do not, which we expect is due to either biological variability or inaccurate estrous stage prediction. Regardless, the stages clearly form a cycle within the PCA, indicating that the stages are transcriptionally distinct (Figure 1K).

For a more granular view, we examined differentially expressed genes (DEGs) between subsequent cycle stages—for example, from diestrus to proestrus; proestrus to estrus; estrus to metestrus; and metestrus to diestrus. At most cycle comparisons, we identified hundreds of DEGs. Between diestrus-proestrus, 361 genes are downregulated and 506 are upregulated (Figure 1L). Between proestrus-estrus, 459 genes are downregulated and 769 genes are upregulated (Figure 1M). Between estrus-metestrus, 438 genes are downregulated and 242 genes are upregulated (Figure 1N). Finally, between metestrus-diestrus, 100 genes are downregulated and 45 genes are upregulated (Figure 1O).

To better visualize the cyclical changes in DEGs, we plotted the top 15 enriched DEGs of each cycle stage in a heatmap, showing a cascade of gene expression during the estrous cycle (Figure 1P). This highly dynamic transcriptional landscape of the cycling uterus provides a rich dataset with which to explore the molecular mechanics that may link hormone cycles to cyclical morphogenesis in the uterus.

Genes associated with embryonic development are cyclically expressed in the adult mouse uterus during the estrous cycle

We were curious if the DEGs at each cycle transition were enriched in particular gene classes, so we performed Gene Ontology (GO) analysis.[20] Curiously, developmental biology GO terms were prevalent at metestrus. The top GO terms included limb development; appendage development; limb morphogenesis; appendage morphogenesis; tube development; and embryonic limb morphogenesis (Figure 2C). At proestrus, the top GO terms included sensory perception of smell; sterol biosynthetic process; and epithelium development (Figure 2A). At estrus, the top GO terms included response to external stimulus and response to other organism (Figure 2B).

Using the GO term analysis as a partial guide, we manually curated the developmental genes and signaling pathways that were differentially expressed in the uterus across the estrous cycle and assembled heatmaps and a table (Table S2) showing differential gene expression. For example, Hox family genes that have known roles in implantation[21–24] such as *Hoxa10, Hoxa11, Hoxd11*, and *Msx1* were all upregulated when progesterone is high during metestrus and diestrus (Figure 2D; Table S2). Conversely, HoxB4 is known to be expressed in uterine glandular epithelial cells,[25] and we found *Hoxb4* to be cyclically expressed with higher expression in early stages when gland numbers peak (Figures 1I and 2D; Table S2).

Likewise, dynamic expression of Wnt ligands has been suggested during the estrous cycle,[26] with *Wnt7b* being required for uterine gland development.[27,28] Notably, we found *Wnt7b* also cycled with higher expression during the early stages (Figure 2E; Table S2), while *Wnt11* and several Wnt signaling transducers displayed the converse pattern, peaking late in the cycle (Figure 2E; Table S2). Finally, TGF-β signaling is also required for implantation and uterine gland and myometrial development,[29,30] but its role during the estrous cycle is unknown. In our dataset, we identified differential expression of genes involved in TGF-β signaling: *Tgfbi* is enriched at metestrus and diestrus, while *Lrg1* is enriched at estrus (Figure 2F; Table S2). Thus, the expression of many of genes required for either implantation or uterine development are dynamically expressed across the estrous cycle, though the relationship between this cyclical expression and cyclical uterine remodeling has yet to be determined.

Hedgehog signaling components are cyclically co-regulated across the estrous cycle

Our most striking finding was that the genes encoding nearly all members of Hedgehog signaling pathway (Figure 3A) were cyclically expressed together and enriched at diestrus (Figures 3B–3M; Table S2). The major Hh ligand in the uterus, *Ihh*, and the known downstream target genes of the pathway, such as *Gli1* and *Ptch1*, are significantly enriched (denoted with an asterisk) (Figure 3B; Table S2). Given that *Ihh* is a direct target of progesterone at implantation,[8,10,31] enrichment of *Ihh* and downstream target genes *Gli1* and *Ptch1* at metestrus

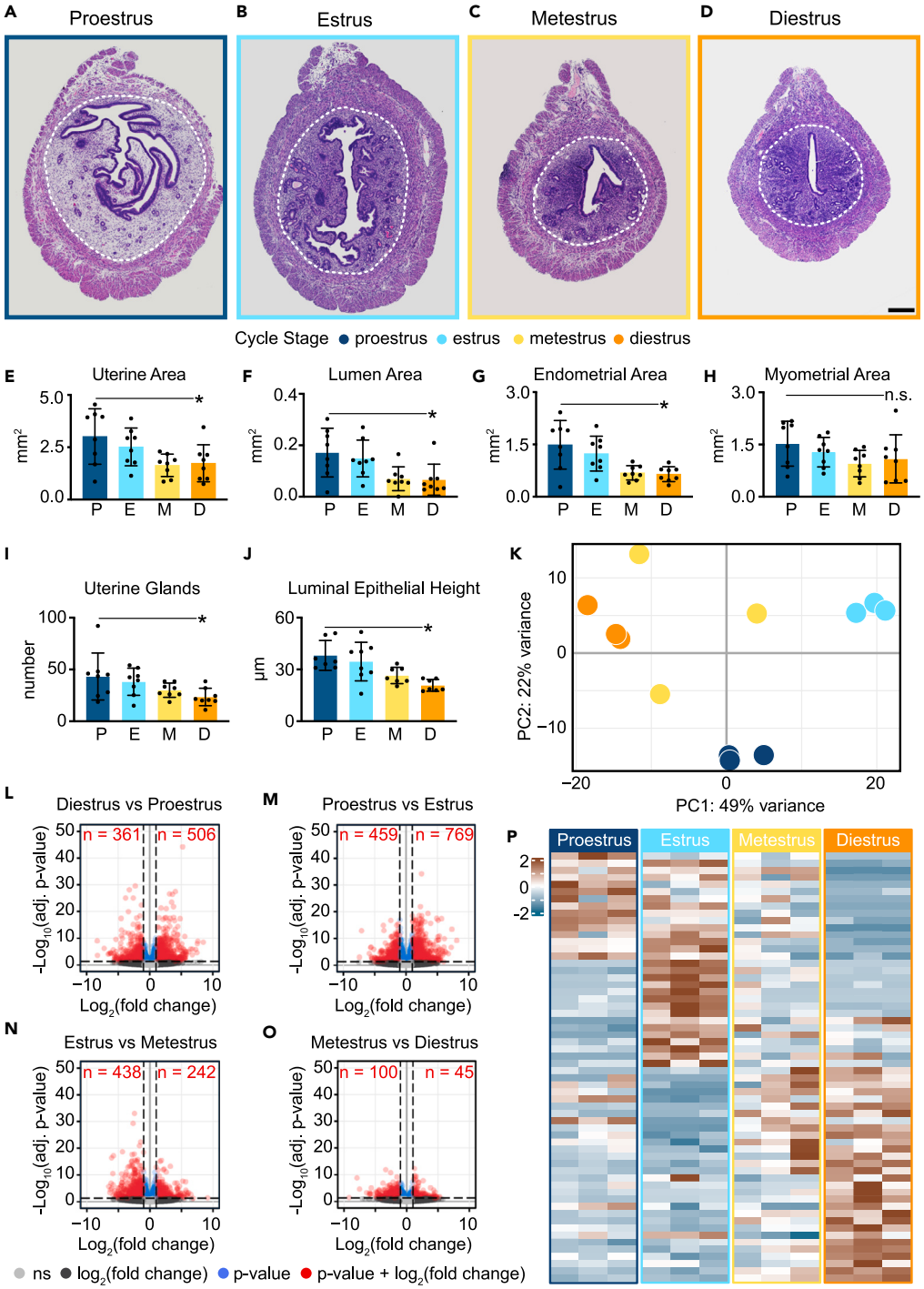

Figure 1. Cyclical mouse uterine remodeling occurs concomitant with transcriptional changes

(A–J) H&E staining of mouse uterine sections at (A) proestrus, (B) estrus, (C) metestrus, and (D) diestrus where the dotted white line denotes boundary between the endometrium and myometrium. Scale bar = 250µm. Quantitation of (E) uterine area, (F) lumen area, (G) endometrial area, (H) myometrial area, (I) uterine gland number, and (J) luminal epithelial height during those same time points. Each point on the graphs represents one uterus and is the mean quantification of 4 or more sections; all error bars are standard deviation of the mean.

(K–O) (K) Principal-component analysis (PCA) plot of 3′ TagSeq dataset. Volcano plots showing differential gene expression between (L) diestrus and proestrus, (M) proestrus and estrus, (N) estrus and metestrus, and (O) metestrus and diestrus.

(P) Heatmap of the most variable differentially expressed genes at each estrous cycle stage, where each column represents one sample. All heatmaps use z-scores of the DESeq2 variance stabilized counts. t tests were performed, where * = $p < 0.05$; n.s. = not significant.

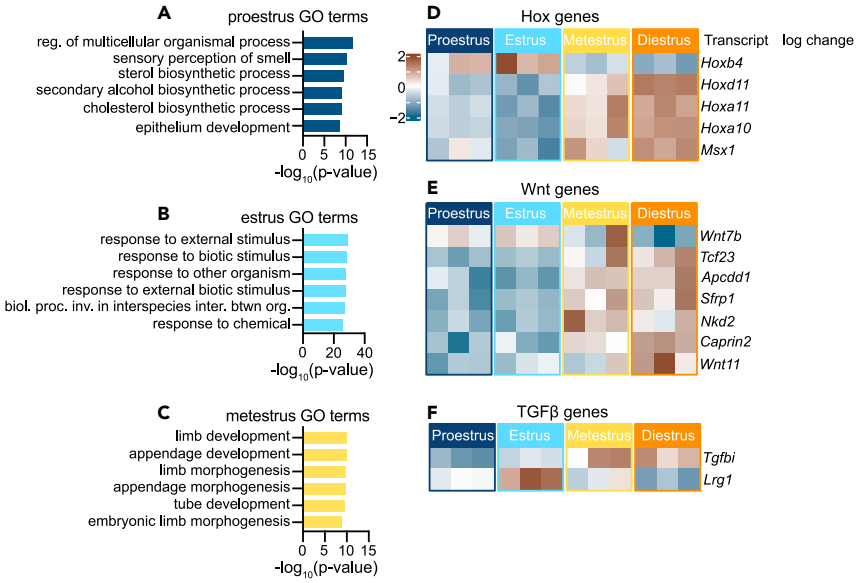

Figure 2. Development genes are cyclically expressed in the uterus during the estrous cycle

(A–F) GO terms of differentially expressed genes enriched at (A) proestrus, (B) estrus, and (C) metestrus. Heatmaps of (D) Hox genes, (E) Wnt signaling, and (F) TGF-β signaling. See also Table S2. Each column represents one sample, and all heatmaps use z-scores of the DESeq2 variance stabilized counts.

or diestrus when progesterone is high was expected.[4] However, the remaining signaling components, including *Gli2*, *Gli3*, *Ptch2*, *Smo*, *Sufu*, *Gpr161*, *Kif7*, *Evc*, and *Evc2* are not typical downstream targets of Hh signaling, yet they also trend upward or are significantly enriched (denoted with an asterisk) at diestrus (Figure 3B; Table S2). We confirmed the significant enrichment of most of these genes by qPCR on an additional 5 animals for a total of n = 8 (Figures 3C–3M). When evaluated with n = 8, some of the pathway components differ from the RNA-seq dataset (Figures 3E–G, 3I, and 3L). Thus, uterine expression of the genes encoding most of the Hh signaling are co-regulated across the mouse estrous cycle.

Hedgehog signaling is required for iterative uterine remodeling across the estrous cycle

While Hedgehog signaling has been extensively studied at implantation, specifically in the endometrium, less is known about possible roles for Hedgehog signaling in uterine remodeling or homeostasis across the normal estrous cycle. We therefore made a conditional knockout of the major activator, *smoothened* (*Smo*), using the *progesterone receptor cre* (*PR-Cre*, Figure 4A) which is expressed throughout the adult uterus.[32,33] The controls (ctrl) were *PR-Cre*$^{+/-\ or\ -/-}$ *Smo*$^{fl/+\ or\ +/+}$, and the conditional knockouts (*Smo* cKO) were *PR-Cre*$^{+/-}$ *Smo*$^{fl/fl}$. We confirmed that *Smo* is indeed significantly decreased or absent in the cKOs compared to the controls by qPCR (Figure 4B). *Smo* is the major activator of the Hh signaling pathway; therefore, the *Smo* cKOs should not be able to activate downstream Hh signaling target genes. We confirmed this by checking for the expression of *Gli1*, a downstream target gene of the pathway. Indeed, while *Gli1* is upregulated at diestrus compared to estrus in our controls, that fails to occur in the cKOs (Figure 4C). In addition to looking at the expression of *Smo* and *Gli1*, we also looked at fertility because previous work has shown that Hedgehog signaling is required for implantation.[10,31,34–36] To confirm that our cKO is infertile, we performed breeding studies on the controls and *Smo* cKOs. The control mice had an average of 9 pups per litter, while the *Smo* cKOs failed to ever have pups (Figure 4D). We also confirmed that the *Smo* cKO animals cycled normally compared to controls using three methods. With vaginal cytology, we found that the cKOs progress through the estrous cycle relatively normally, albeit with a significantly shorter diestrus stage (Figure 4E). We also looked at levels of progesterone in the serum with the University of Virginia Ligand Assay and Analysis Core and showed no significant difference between controls and cKOs (Figure S1A). Finally, we show that both controls and *Smo* cKO ovaries have corpus lutea at diestrus, suggesting that ovulation is occurring in all animals (Figure S1B).

Despite this relatively normal cycling, uteri lacking Smo displayed radically altered morphologies (Figures 4F–4I). Smo cKO uteri failed to thicken during the estrogen-dominant early stages of the cycle (i.e., estrus). Measurement of both the total uterine area and the endometrial area confirmed this result as both were significantly reduced in the mutants (Figures 4F, 4G, 4J, and 4K). Thus, Hedgehog signaling is required for normal morphogenetic changes in the uterine endometrium across the mouse estrus cycle.

Hedgehog signaling controls homeostasis of longitudinal smooth muscle in the uterus

In contrast to the obvious endometrial phenotype at estrus, *Smo* cKO mice displayed a more subtle but interesting phenotype during the progesterone-dominant later stages (i.e., diestrus), when the endometrium is normally quite thin (see Figure 1). Specifically, the size of the myometrium, composed of inner circular and outer longitudinal layers of muscle,[37] was increased relative to the endometrium in *Smo*

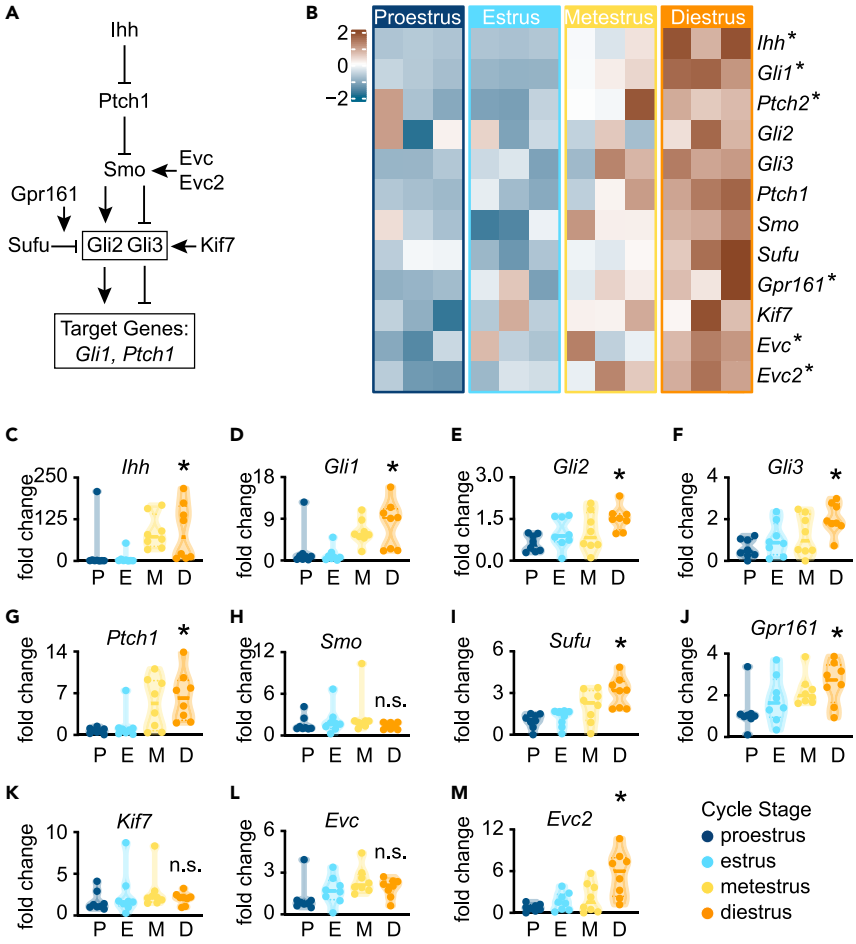

Figure 3. The Hedgehog signaling pathway is cyclically regulated across the estrous cycle

(A) The biochemical pathway of Hh signaling.

(B) Heatmap of the core components of Hh signaling across the estrous cycle, where the *Z* score of the DESeq2 variance stabilized counts is used. Each column represents one sample. See also Table S2.

(C–M) qPCR of the same core components of Hh signaling with n = 8 samples. See also Table S1. t tests were performed, where * = $p < 0.05$; n.s. = not significant.

cKO mice (Figure 4L). Moreover, the appearance of the tissue was altered, seemingly thrown into aberrant deformations not observed in control uteri (Figure 5). This stage-specific change in the myometrium was surprising as the myometrial area does not remodel across the cycle in normal mice (see Figure 1).

This result prompted us to further quantify these myometrial phenotypes. We found that while the *Smo* cKO longitudinal smooth muscle layer trended toward increased thickness at diestrus, it did not reach statistical significance (Figure 5A). However, when we quantified deformation using "smoothness" (i.e., ratio of uterine perimeter length [Figure 5B′) to circumference of the best fit ellipse [Figure 5B″]), we observed a significant decrease specifically at diestrus in the *Smo* cKO (Figures 5C–5F). These data suggest that in the absence of Hh signaling the mouse uterus undergoes aberrant deformation of the outer muscular layer.

Muscle fibers are larger in the absence of Smoothened

The aberrant tissue deformation observed in the myometrium of *Smo* cKO at diestrus is reminiscent of normal folding observed in some developing organs, such as the exterior of some mammalian brains. There is evidence that such folding results from differential growth of the outer gray matter and the inner white matter, resulting in mechanical buckling.[38] The inverse is true in the developing vertebrate gut, where the growing inner endoderm and mesenchyme are restrained by the outer layers of smooth muscle resulting in folding.[39] We hypothesized that the aberrant deformation of uterine smooth muscles in the *Smo* cKO at diestrus may be caused by an increase in longitudinal muscle fiber number or size compared to the relatively unchanging endometrial area (Figure 4L).

We therefore quantified the size and number of muscle fibers using Masson Trichrome histology, which stains muscle in red and collagen in blue (histology in Figures 5 and 6). Given that uterine smooth muscle fibers are embedded in extracellular matrix,[40] we were able to assess smooth muscle fibers using Ilastik, which takes advantage of color and texture differences to differentiate structures,[41] to produce masks of

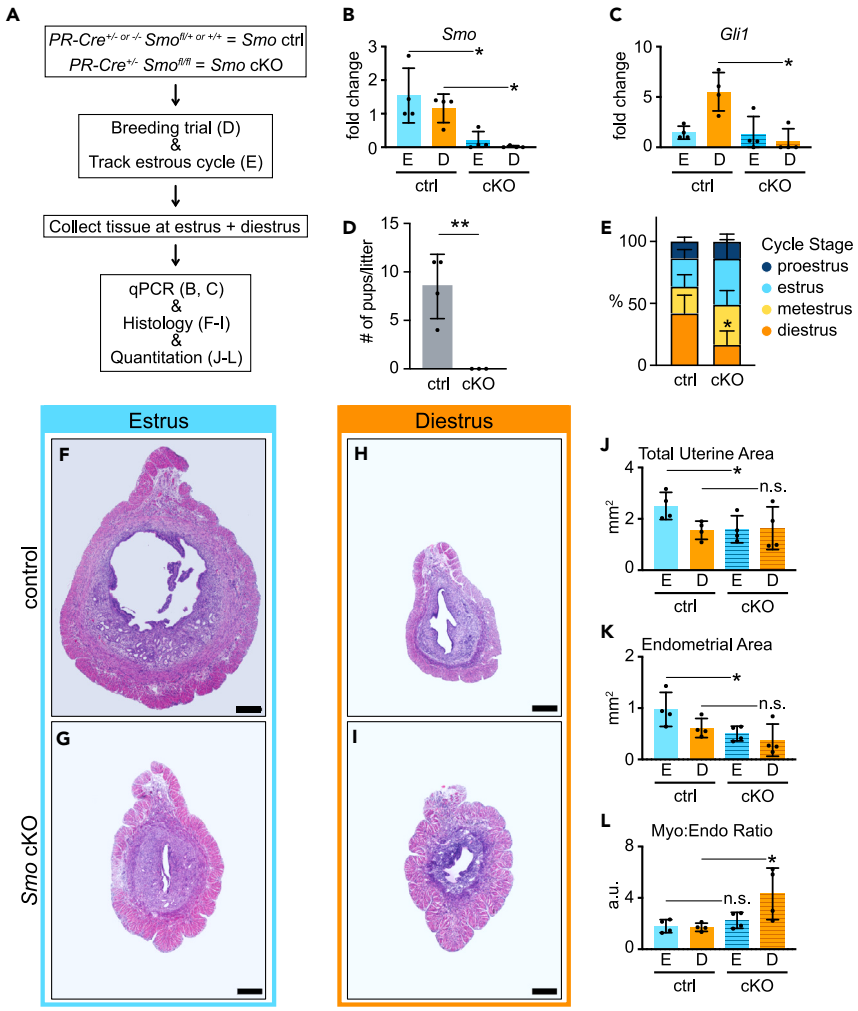

Figure 4. Hedgehog signaling is required for cyclical uterine remodeling

(A) Experimental flow to determine role of Hh signaling in the adult uterus during the estrous cycle.

(B) qPCR for *Smoothened* in the controls and *Smo* cKOs.

(C) qPCR for *Gli1* in the controls and *Smo* cKOs.

(D) Breeding trial of controls and *Smo* cKOs.

(E) Estrous cyclicity of controls and *Smo* cKOs.

(F–I) H&E-stained uterine sections from control and *Smo* cKOs.

(J–L) Quantitation of (J) total uterine area, (K) endometrial area, and (L) myometrial-to-endometrial area ratio. Each point on the graphs represents one uterus and is the mean quantification of 4 or more sections. t tests were performed, where * = $p < 0.05$; n.s. = not significant. Scale in image = 250μm. All error bars are standard deviation of the mean.

muscle fibers (Figures 6A–6D and 6A′′–6D′′). While the average number of muscle fibers was unchanged, we observed a striking and significant increase in the size of individual muscle fibers in *Smo* cKO uteri, specifically at diestrus (Figures 6E and 6F). A more granular view of the data revealed a curious pattern to this effect. When we binned fibers by area, we found that the *Smo* cKO phenotype was driven by changes in fibers at the extremes of size (Figure 6G). These data suggest that changes in muscle fiber size may underlie the aberrant deformation of the uterine myometrium that accompanies loss of Hedgehog signaling in the cycling adult mouse uterus.

DISCUSSION

One of the first studies to show that the human uterus undergoes cyclical remodeling (rather than pathological changes) during the menstrual cycle was published in 1908.[42] Since then, a large body of literature has characterized this regenerative process and has focused on understanding menstruation as well as timing of re-epithelialization of the uterus.[43–48] However, it would be nearly 100 years before a similar study on mouse uterine remodeling relative to circulating steroid hormone levels was published,[4] despite this animal's power and widespread use as a tractable genetic model for mammalian biology.

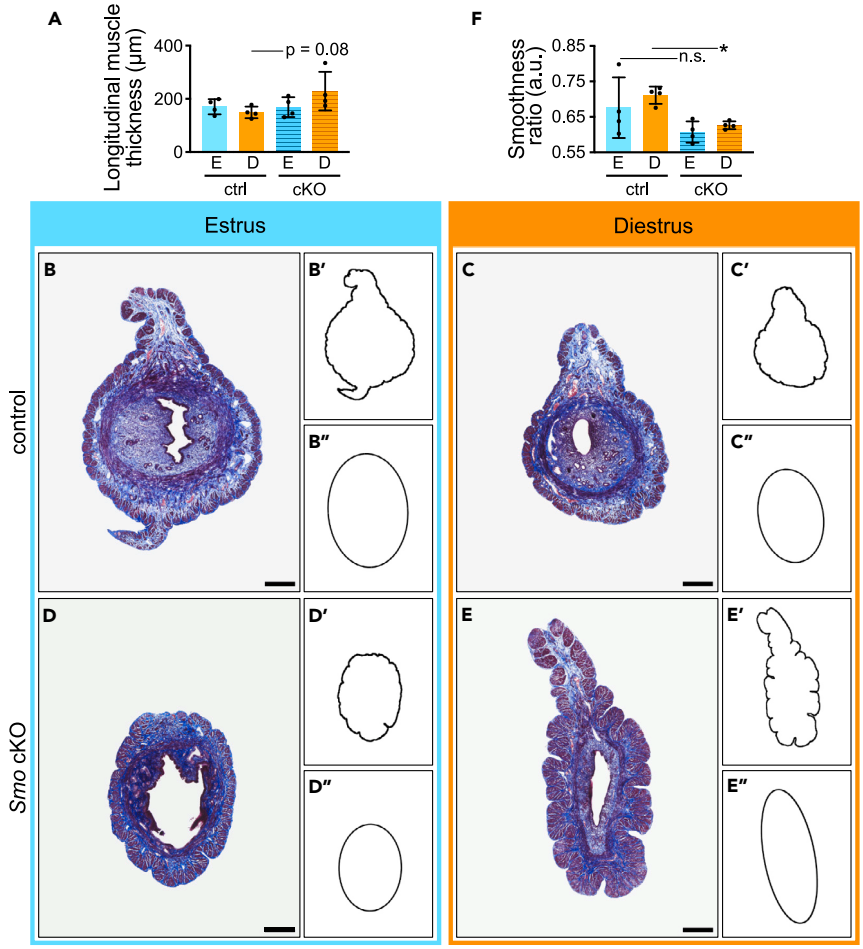

Figure 5. The myometrium is significantly folded in the absence of Smoothened

(A–E) (A) Quantitation of longitudinal muscle thickness. Each point on the graph represents one uterus and is the mean quantification of 4 or more sections. (B–E) Masson Trichrome histology of the mouse uterus. (B′–E′) Outline of sections highlighting the ruffled nature of the *Smo* cKO. (B″–E″) Best fit ellipse of the outline. (F) The smoothness of each sample was determined by taking the ratio of the true outline to the best fit ellipse. Each point on the graph represents one uterus and is the mean quantification of 4 or more sections. t tests were performed, where * = $p < 0.05$; n.s. = not significant. Scale bar = 250μm. All error bars are standard deviation of the mean.

In addition, mouse models have been used extensively to understand the impact of estrogen and progesterone on the uterus, but almost exclusively by exogenously administered hormones to ovariectomized mice,[49,50] genetically modified mice to examine loss of steroid hormone signaling,[7,51–53] or at implantation.[10,54–58] By contrast, the normally cycling mouse uterus remains far less understood. Several studies have assessed morphological changes across the estrous cycle,[3,4] and others have compared the transcriptomes of two cycle stages.[12,13] However, as Wood et al. remarked, several parameters in their study showed correlations with specific estrous cycle stages.[4] Therefore, we wanted to expand the transcriptional landscape of the cycling uterus.

We determined the cyclical transcriptome of the whole uterus across the four key stages of the estrous cycle. We found that hundreds of genes are differentially expressed at each cycle stage comparison, demonstrating that the mouse uterus is highly transcriptionally dynamic across the relative short span of 24 h, which roughly characterized each stage (Figure 1). This result contrasts sharply with the mouse oviduct, which we recently showed undergoes minimal transcriptional change across the estrous cycle.[59]

Among the most interesting results of this analysis was that many developmental pathways are differentially expressed across the estrous cycle, including Hox genes, Wnt signaling, and TGF-β signaling (Figure 2) and Indian Hedgehog signaling (Figure 3). *Ihh* is a direct target of progesterone signaling at implantation[8,10] and has also been identified as differentially expressed between proestrus and estrus,[12] and estrus and diestrus.[13] Therefore, *Ihh* itself was a positive control in our dataset. However, it was striking to us that most of the system, including receptors and transducers, displayed a clear cycle of expression peaking at diestrus (Figure 3). And while Hh signaling is required for uterine development[60] and implantation,[10] a role in the cycling uterus has not been described.

We took a conditional genetic approach, which revealed a key role for Hh signaling in uterine remodeling and homeostasis across the normal estrous cycle. Conditional deletion of *smoothened* with the *progesterone receptor Cre* resulted in a failure of endometrial expansion

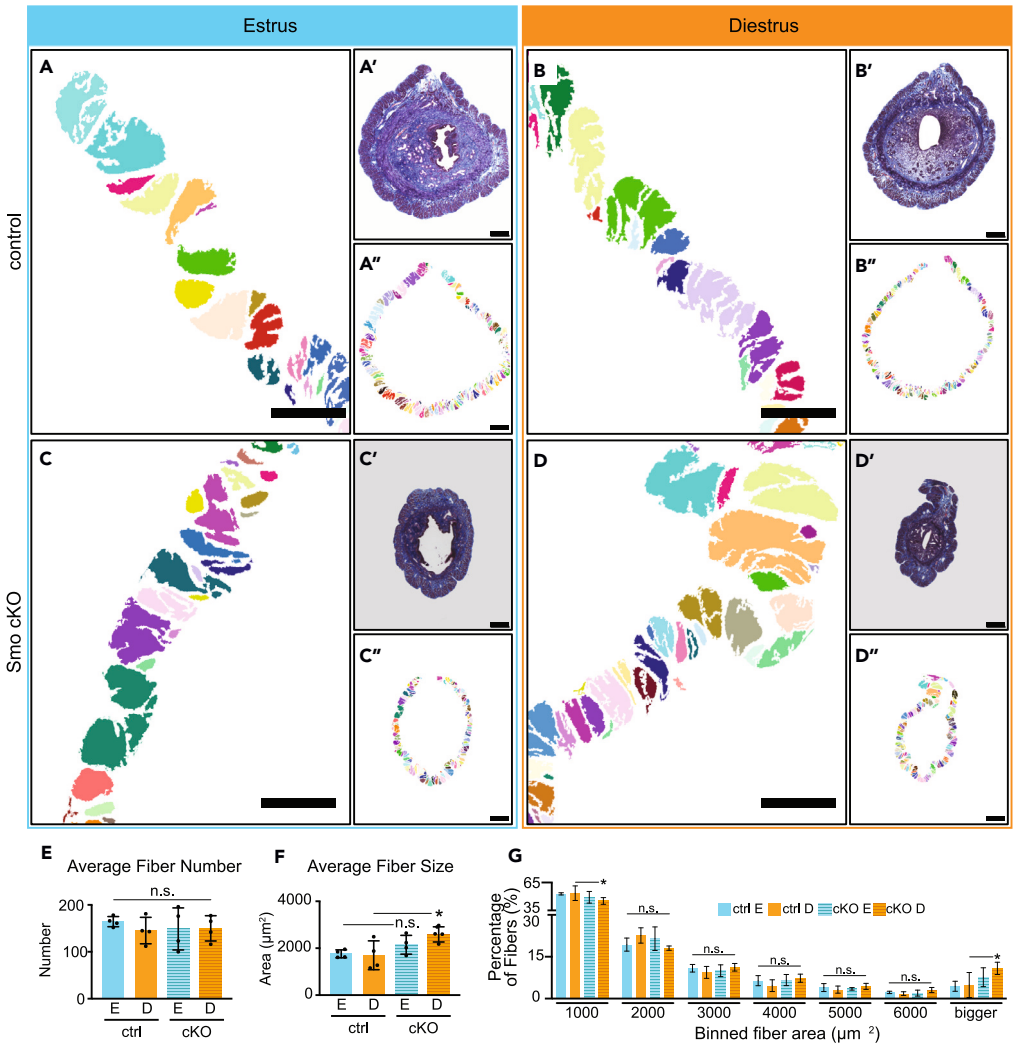

Figure 6. Myometrial fibers are significantly bigger in the absence of Smoothened

(A–D) Masks of the longitudinal muscle fibers were produced using Ilastik. (A′–D′) Masson Trichrome histology was used to identify the myometrial muscle fibers. (A″–D″) Longitudinal fibers were identified throughout the entire section.

(E–G) (E) Quantitation of the fiber number in each sample. Each point on the graph represents one uterus and is the mean quantification of 4 or more sections. (F) Quantitation of the fiber area in each sample. Each point on the graph represents one uterus and is the mean quantification of 4 or more sections. (G) Fiber areas were binned in 1000μm^2 increments. t tests were performed, where * = $p < 0.05$ and n.s. = not significant. Scale in main image = 50μm. Scale in 'and "images = 250μm. All error bars are standard deviation of the mean.

during estrus (Figure 4). We found it curious that the upregulation in gene expression was at diestrus and yet the endometrial phenotype was at estrus. We speculate that progesterone-regulated Hh signaling primes the endometrium for the remodeling that occurs under estrogen. In support of this speculation, it has recently been shown in human endometrial biopsies that the progesterone receptor binds the *Ihh* promoter during the proliferative phase of the menstrual cycle, when estrogen is high.[14] Finally, while the underlying basis for this phenotype remains to be discovered, it is of special interest because Ihh signaling is required for endometrial stromal cell proliferation to support implantation in the pregnant uterus.[10]

In addition to this failure of endometrial remodeling, loss of *Smo* also severely disrupted the homeostasis of the myometrium. This muscular layer normally changes very little across the cycle (Figure 1), but in the absence of Hh signaling, we observed aberrant deformation accompanied by an increase in muscle fiber size (Figures 5 and 6). Whether this increase in fiber size is due to hyperplasia or hypertrophy remains to be determined, but the results are important because Hh signaling also governs smooth muscle differentiation during development and homeostasis in other organs.[61–67] Moreover, the deformed appearance of the myometrium of *Smo* cKO mice at diestrus is remarkably similar to that observed in H&E-stained post-partum mouse uteri which are undergoing involution, or the healing process after birth by which the myometrium remodels to return to a non-pregnant state.[68] Our hypothesis moving forward is that Hh signaling in the myometrium is downstream of progesterone signaling (similar to the endometrium at implantation) and is required for myometrial quiescence. This is

supported in part by the role progesterone plays in myometrial quiescence during pregnancy.[69–71] In the future, we will investigate the role of Hh signaling in myometrial quiescence and remodeling that occurs during late pregnancy or involution.

Finally, our data provide another lens through which to view the general phenomenon of cyclical patterns of gene expression. Such cycles are most well defined in the context of circadian rhythm[1] but control diverse biological processes in adults and in embryos. Interestingly, Hedgehog signaling has been implicated in the hair growth cycle in adult mammals[72,73] and many Hh-related genes display long (seasonal) cycles of gene expression.[74,75] On shorter time scales, elements of the Hh signaling pathway also display daily cycles of expression in the adult mouse liver that are linked to circadian rhythm.[76] Our data therefore shed new light on important aspects of the reproductive cell biology of uterine remodeling and also more generally on the issue of cyclical control of gene expression.

Limitations of the study

There are several caveats to the work presented here. The *PGR-Cre* line is expressed in additional tissues including the ovary, oviduct, hypothalamus, and pituitary. While we cannot rule out their involvement in our phenotype, the *smo* cKO mice do cycle normally based on vaginal cytology which indicates that estrogen and progesterone are being cyclically secreted, progesterone is secreted at concentrations similar to controls, and the *smo* cKO ovary shows corpus lutea similar to controls demonstrating that ovulation is occuring. We performed transverse sectioning instead of sagittal sectioning. This precludes us from assessing the entire length of the uterus. To overcome the limitations of this, we quantified at least four sections from over 500 μm along the length of the uterus. Finally, we performed bulk RNA-seq on the whole uterus. The main limitation here is that we do not have single-cell resolution and have missed potential gene expression changes (i.e., if one cell type downregulates a signaling pathway, but another cell type upregulates it, we have likely not identified either change in our dataset).

STAR★METHODS

Detailed methods are provided in the online version of this paper and include the following:

- KEY RESOURCES TABLE
- RESOURCE AVAILABILITY
  - Lead contact
  - Materials availability
  - Data and code availability
- EXPERIMENTAL MODEL AND STUDY PARTICIPANT DETAILS
  - Mice
- METHOD DETAILS
  - Progesterone assay
  - Tissue processing, histology, and immunofluorescence
  - RNA isolation and cDNA synthesis
  - qPCR
  - TagSeq
  - Sequence data pre-processing
- QUANTIFICATION AND STATISTICAL ANALYSIS
  - Image quantitation
  - TagSeq data analysis

SUPPLEMENTAL INFORMATION

Supplemental information can be found online at https://doi.org/10.1016/j.isci.2023.107993.

ACKNOWLEDGMENTS

The authors are deeply grateful to the staff of the Genomic Sequencing and Analysis Facility (RRID:SCR_021713) and the Animal Resource Facility at the University of Texas at Austin, as well at the University of Virginia Center for Research in Reproduction Ligand Assay and Analysis core, which is supported by the Eunice Kennedy Shriver NICHD Grant R24 HD102061. We would also like to thank Dr. Carmen Williams, Dr. Stephen Vokes, and the members of the Wallingford lab for critical scientific discourse relevant to the data presented here. Part of the graphical abstract was created with BioRender. This work was supported by the NIH/NICHD: F32HD095618 (E.C.R.) and R01HL117164 and R01HD085901 (J.B.W.). This work was also supported by the University of Texas at Austin Undergraduate Research Fellowships (K.T. and H.M.).

AUTHOR CONTRIBUTIONS

E.C.R.: Conceptualization, Methodology, Investigation, Data curation, Formal Analysis, Visualization, Writing, Supervision, Project Administration. **N.K.T.**: Investigation, Validation. **A.N.G.**: Investigation, Validation. **H.M.**: Investigation, Validation. **M.N.**: Investigation, Validation.

T.R.: Investigation, Validation. E.U.: Investigation, Validation. L.B.: Investigation, Validation. R.D.F.: Investigation. J.B.W.: Conceptualization, Writing – Review & Editing, Supervision, Funding Acquisition, Project Administration.

DECLARATION OF INTERESTS

The authors declare no competing interests.

INCLUSION AND DIVERSITY

We support inclusive, diverse, and equitable conduct of research.

Received: February 20, 2023
Revised: August 24, 2023
Accepted: September 16, 2023
Published: September 20, 2023

REFERENCES

1. Doherty, C.J., and Kay, S.A. (2010). Circadian control of global gene expression patterns. Annu. Rev. Genet. *44*, 419–444. https://doi.org/10.1146/annurev-genet-102209-163432.
2. Hubaud, A., and Pourquié, O. (2014). Signalling dynamics in vertebrate segmentation. Nat. Rev. Mol. Cell Biol. *15*, 709–721. https://doi.org/10.1038/nrm3891.
3. Jin, S. (2019). Bipotent stem cells support the cyclical regeneration of endometrial epithelium of the murine uterus. Proc. Natl. Acad. Sci. USA *116*, 6848–6857. https://doi.org/10.1073/pnas.1814597116.
4. Wood, G.A., Fata, J.E., Watson, K.L.M., and Khokha, R. (2007). Circulating hormones and estrous stage predict cellular and stromal remodeling in murine uterus. Reproduction *133*, 1035–1044. https://doi.org/10.1530/REP-06-0302.
5. Spooner-Harris, M., Kerns, K., Zigo, M., Sutovsky, P., Balboula, A., and Patterson, A.L. (2023). A re-appraisal of mesenchymal-epithelial transition (MET) in endometrial epithelial remodeling. Cell Tissue Res. *391*, 393–408. https://doi.org/10.1007/s00441-022-03711-z.
6. Winkler, I., Tolkachov, A., Lammers, F., Lacour, P., Schneider, N., Koch, M.-L., Panten, J., Grünschläger, F., Daugelaite, K., Poth, T., et al. (2022). The function and decline of the female reproductive tract at single-cell resolution. Preprint at bioRxiv. https://doi.org/10.1101/2022.10.26.513823.
7. Cheon, Y.P., Li, Q., Xu, X., DeMayo, F.J., Bagchi, I.C., and Bagchi, M.K. (2002). A genomic approach to identify novel progesterone receptor regulated pathways in the uterus during implantation. Mol. Endocrinol. *16*, 2853–2871. https://doi.org/10.1210/me.2002-0270.
8. Takamoto, N., Zhao, B., Tsai, S.Y., and DeMayo, F.J. (2002). Identification of Indian hedgehog as a progesterone-responsive gene in the murine uterus. Mol. Endocrinol. *16*, 2338–2348. https://doi.org/10.1210/me.2001-0154.
9. Jeong, J.W., Lee, K.Y., Kwak, I., White, L.D., Hilsenbeck, S.G., Lydon, J.P., and DeMayo, F.J. (2005). Identification of murine uterine genes regulated in a ligand-dependent manner by the progesterone receptor. Endocrinology *146*, 3490–3505. https://doi.org/10.1210/en.2005-0016.
10. Lee, K., Jeong, J., Kwak, I., Yu, C.T., Lanske, B., Soegiarto, D.W., Toftgard, R., Tsai, M.J., Tsai, S., Lydon, J.P., and DeMayo, F.J. (2006). Indian hedgehog is a major mediator of progesterone signaling in the mouse uterus. Nat. Genet. *38*, 1204–1209. https://doi.org/10.1038/ng1874.
11. Wei, Q., Levens, E.D., Stefansson, L., and Nieman, L.K. (2010). Indian Hedgehog and its targets in human endometrium: menstrual cycle expression and response to CDB-2914. J. Clin. Endocrinol. Metab. *95*, 5330–5337. https://doi.org/10.1210/jc.2010-0637.
12. Yip, K.S., Suvorov, A., Connerney, J., Lodato, N.J., and Waxman, D.J. (2013). Changes in mouse uterine transcriptome in estrus and proestrus. Biol. Reprod. *89*, 13. https://doi.org/10.1095/biolreprod.112.107334.
13. Zhou, Y., Yan, H., Liu, W., Hu, C., Zhou, Y., Sun, R., Tang, Y., Zheng, C., Yang, J., and Cui, Q. (2022). A multi-tissue transcriptomic landscape of female mice in estrus and diestrus provides clues for precision medicine. Front. Cell Dev. Biol. *10*, 983712. https://doi.org/10.3389/fcell.2022.983712.
14. Chi, R.P.A., Wang, T., Adams, N., Wu, S.P., Young, S.L., Spencer, T.E., and DeMayo, F. (2020). Human Endometrial Transcriptome and Progesterone Receptor Cistrome Reveal Important Pathways and Epithelial Regulators. J. Clin. Endocrinol. Metab. *105*, e1419–e1439. https://doi.org/10.1210/clinem/dgz117.
15. Garcia-Alonso, L., Handfield, L.F., Roberts, K., Nikolakopoulou, K., Fernando, R.C., Gardner, L., Woodhams, B., Arutyunyan, A., Polanski, K., Hoo, R., et al. (2021). Mapping the temporal and spatial dynamics of the human endometrium *in vivo* and *in vitro*. Nat. Genet. *53*, 1698–1711. https://doi.org/10.1038/s41588-021-00972-2.
16. Wang, W., Vilella, F., Alama, P., Moreno, I., Mignardi, M., Isakova, A., Pan, W., Simon, C., and Quake, S.R. (2020). Single-cell transcriptomic atlas of the human endometrium during the menstrual cycle. Nat. Med. *26*, 1644–1653. https://doi.org/10.1038/s41591-020-1040-z.
17. Krjutškov, K., Katayama, S., Saare, M., Vera-Rodriguez, M., Lubenets, D., Samuel, K., Laisk-Podar, T., Teder, H., Einarsdottir, E., Salumets, A., and Kere, J. (2016). Single-cell transcriptome analysis of endometrial tissue. Hum. Reprod. *31*, 844–853. https://doi.org/10.1093/humrep/dew008.
18. Talbi, S., Hamilton, A.E., Vo, K.C., Tulac, S., Overgaard, M.T., Dosiou, C., Le Shay, N., Nezhat, C.N., Kempson, R., Lessey, B.A., et al. (2006). Molecular phenotyping of human endometrium distinguishes menstrual cycle phases and underlying biological processes in normo-ovulatory women. Endocrinology *147*, 1097–1121. https://doi.org/10.1210/en.2005-1076.
19. Dodds, K.N., Staikopoulos, V., and Beckett, E.A.H. (2015). Uterine Contractility in the Nonpregnant Mouse: Changes During the Estrous Cycle and Effects of Chloride Channel Blockade. Biol. Reprod. *92*, 141. https://doi.org/10.1095/biolreprod.115.129809.
20. Thomas, P.D., Ebert, D., Muruganujan, A., Mushayahama, T., Albou, L.P., and Mi, H. (2022). PANTHER: Making genome-scale phylogenetics accessible to all. Protein Sci. *31*, 8–22. https://doi.org/10.1002/pro.4218.
21. Daikoku, T., Cha, J., Sun, X., Tranguch, S., Xie, H., Fujita, T., Hirota, Y., Lydon, J., DeMayo, F., Maxson, R., and Dey, S.K. (2011). Conditional deletion of Msx homeobox genes in the uterus inhibits blastocyst implantation by altering uterine receptivity. Dev. Cell *21*, 1014–1025. https://doi.org/10.1016/j.devcel.2011.09.010.
22. Nallasamy, S., Li, Q., Bagchi, M.K., and Bagchi, I.C. (2012). Msx homeobox genes critically regulate embryo implantation by controlling paracrine signaling between uterine stroma and epithelium. PLoS Genet. *8*, e1002500. https://doi.org/10.1371/journal.pgen.1002500.
23. Nallasamy, S., Kaya Okur, H.S., Bhurke, A., Davila, J., Li, Q., Young, S.L., Taylor, R.N., Bagchi, M.K., and Bagchi, I.C. (2019). Msx Homeobox Genes Act Downstream of BMP2 to Regulate Endometrial Decidualization in Mice and in Humans. Endocrinology *160*, 1631–1644. https://doi.org/10.1210/en.2019-00131.
24. Lim, H., Ma, L., Ma, W.G., Maas, R.L., and Dey, S.K. (1999). Hoxa-10 regulates uterine stromal cell responsiveness to progesterone during implantation and decidualization in the mouse. Mol. Endocrinol. *13*, 1005–1017. https://doi.org/10.1210/mend.13.6.0284.
25. AlKusayer, G.M., Pon, J.R., Peng, B., Klausen, C., Lisonkova, S., Kinloch, M., Yong, P., Muhammad, E.M.S., Leung, P.C.K., and Bedaiwy, M.A. (2018). HOXB4 Immunoreactivity in Endometrial Tissues From Women With or Without Endometriosis. Reprod. Sci. *25*, 950–957. https://doi.org/10.1177/1933719117732164.
26. Miller, C., Pavlova, A., and Sassoon, D.A. (1998). Differential expression patterns of Wnt

genes in the murine female reproductive tract during development and the estrous cycle. Mech. Dev. *76*, 91–99. https://doi.org/10.1016/s0925-4773(98)00112-9.

27. Miller, C., and Sassoon, D.A. (1998). Wnt-7a maintains appropriate uterine patterning during the development of the mouse female reproductive tract. Development *125*, 3201–3211. https://doi.org/10.1242/dev.125.16.3201.
28. Hayashi, K., Yoshioka, S., Reardon, S.N., Rucker, E.B., Spencer, T.E., DeMayo, F.J., Lydon, J.P., and MacLean, J.A. (2011). WNTs in the neonatal mouse uterus: potential regulation of endometrial gland development. Biol. Reprod. *84*, 308–319. https://doi.org/10.1095/biolreprod.110.088161.
29. Gao, Y., Duran, S., Lydon, J.P., DeMayo, F.J., Burghardt, R.C., Bayless, K.J., Bartholin, L., and Li, Q. (2015). Constitutive activation of transforming growth factor Beta receptor 1 in the mouse uterus impairs uterine morphology and function. Biol. Reprod. *92*, 34. https://doi.org/10.1095/biolreprod.114.125146.
30. Ni, N., Gao, Y., Fang, X., Melgar, M., Vincent, D.F., Lydon, J.P., Bartholin, L., and Li, Q. (2018). Glandular defects in the mouse uterus with sustained activation of TGF-beta signaling is associated with altered differentiation of endometrial stromal cells and formation of stromal compartment. PLoS One *13*, e0209417. https://doi.org/10.1371/journal.pone.0209417.
31. Wang, X., Li, X., Wang, T., Wu, S.P., Jeong, J.W., Kim, T.H., Young, S.L., Lessey, B.A., Lanz, R.B., Lydon, J.P., and DeMayo, F.J. (2018). SOX17 regulates uterine epithelial-stromal cross-talk acting via a distal enhancer upstream of Ihh. Nat. Commun. *9*, 4421. https://doi.org/10.1038/s41467-018-06652-w.
32. Yang, C.F., Chiang, M.C., Gray, D.C., Prabhakaran, M., Alvarado, M., Juntti, S.A., Unger, E.K., Wells, J.A., and Shah, N.M. (2013). Sexually dimorphic neurons in the ventromedial hypothalamus govern mating in both sexes and aggression in males. Cell *153*, 896–909. https://doi.org/10.1016/j.cell.2013.04.017.
33. Soyal, S.M., Mukherjee, A., Lee, K.Y.S., Li, J., Li, H., DeMayo, F.J., and Lydon, J.P. (2005). Cre-mediated recombination in cell lineages that express the progesterone receptor. Genesis *41*, 58–66. https://doi.org/10.1002/gene.20098.
34. Franco, H.L., Lee, K.Y., Rubel, C.A., Creighton, C.J., White, L.D., Broaddus, R.R., Lewis, M.T., Lydon, J.P., Jeong, J.W., and DeMayo, F.J. (2010). Constitutive activation of smoothened leads to female infertility and altered uterine differentiation in the mouse. Biol. Reprod. *82*, 991–999. https://doi.org/10.1095/biolreprod.109.081513.
35. Harman, R.M., Cowan, R.G., Ren, Y., and Quirk, S.M. (2011). Reduced signaling through the hedgehog pathway in the uterine stroma causes deferred implantation and embryonic loss. Reproduction *141*, 665–674. https://doi.org/10.1530/REP-10-0468.
36. Franco, H.L., Lee, K.Y., Broaddus, R.R., White, L.D., Lanske, B., Lydon, J.P., Jeong, J.W., and DeMayo, F.J. (2010). Ablation of Indian hedgehog in the murine uterus results in decreased cell cycle progression, aberrant epidermal growth factor signaling, and increased estrogen signaling. Biol. Reprod. *82*, 783–790. https://doi.org/10.1095/biolreprod.109.080259.
37. Brody, J.R., and Cunha, G.R. (1989). Histologic, morphometric, and immunocytochemical analysis of myometrial development in rats and mice: I. Normal development. Am. J. Anat. *186*, 1–20. https://doi.org/10.1002/aja.1001860102.
38. Tallinen, T., Chung, J.Y., Biggins, J.S., and Mahadevan, L. (2014). Gyrification from constrained cortical expansion. Proc. Natl. Acad. Sci. USA *111*, 12667–12672. https://doi.org/10.1073/pnas.1406015111.
39. Shyer, A.E., Tallinen, T., Nerurkar, N.L., Wei, Z., Gil, E.S., Kaplan, D.L., Tabin, C.J., and Mahadevan, L. (2013). Villification: how the gut gets its villi. Science *342*, 212–218. https://doi.org/10.1126/science.1238842.
40. Young, R.C., and Hession, R.O. (1999). Three-dimensional structure of the smooth muscle in the term-pregnant human uterus. Obstet. Gynecol. *93*, 94–99. https://doi.org/10.1016/s0029-7844(98)00345-7.
41. Berg, S., Kutra, D., Kroeger, T., Straehle, C.N., Kausler, B.X., Haubold, C., Schiegg, M., Ales, J., Beier, T., Rudy, M., et al. (2019). ilastik: interactive machine learning for (bio)image analysis. Nat. Methods *16*, 1226–1232. https://doi.org/10.1038/s41592-019-0582-9.
42. Hitschmann, F., and Adler, L. (1908). Uterusschleimhaut des geschlechtsreifen Weibes mit besonderer Berücksichtigung der Menstruation.
43. Garry, R., Hart, R., Karthigasu, K.A., and Burke, C. (2009). A re-appraisal of the morphological changes within the endometrium during menstruation: a hysteroscopic, histological and scanning electron microscopic study. Hum. Reprod. *24*, 1393–1401. https://doi.org/10.1093/humrep/dep036.
44. Ludwig, H., and Spornitz, U.M. (1991). Microarchitecture of the human endometrium by scanning electron microscopy: menstrual desquamation and remodeling. Ann. N. Y. Acad. Sci. *622*, 28–46. https://doi.org/10.1111/j.1749-6632.1991.tb37848.x.
45. Salamonsen, L.A., and Woolley, D.E. (1999). Menstruation: induction by matrix metalloproteinases and inflammatory cells. J. Reprod. Immunol. *44*, 1–27. https://doi.org/10.1016/s0165-0378(99)00002-9.
46. Maybin, J.A., Murray, A.A., Saunders, P.T.K., Hirani, N., Carmeliet, P., and Critchley, H.O.D. (2018). Hypoxia and hypoxia inducible factor-1α are required for normal endometrial repair during menstruation. Nat. Commun. *9*, 295. https://doi.org/10.1038/s41467-017-02375-6.
47. Gaide Chevronnay, H.P., Galant, C., Lemoine, P., Courtoy, P.J., Marbaix, E., and Henriet, P. (2009). Spatiotemporal coupling of focal extracellular matrix degradation and reconstruction in the menstrual human endometrium. Endocrinology *150*, 5094–5105. https://doi.org/10.1210/en.2009-0750.
48. Evans, J., Infusini, G., McGovern, J., Cuttle, L., Webb, A., Nebl, T., Milla, L., Kimble, R., Kempf, M., Andrews, C.J., et al. (2019). Menstrual fluid factors facilitate tissue repair: identification and functional action in endometrial and skin repair. FASEB J *33*, 584–605. https://doi.org/10.1096/fj.201800086R.
49. Lydon, J.P., DeMayo, F.J., Conneely, O.M., and O'Malley, B.W. (1996). Reproductive phenotpes of the progesterone receptor null mutant mouse. J. Steroid Biochem. Mol. Biol. *56*, 67–77. https://doi.org/10.1016/0960-0760(95)00254-5.
50. Hewitt, S.C., and Korach, K.S. (2000). Progesterone action and responses in the alphaERKO mouse. Steroids *65*, 551–557. https://doi.org/10.1016/s0039-128x(00)00113-6.
51. Lee, K., Jeong, J., Tsai, M.J., Tsai, S., Lydon, J.P., and DeMayo, F.J. (2006). Molecular mechanisms involved in progesterone receptor regulation of uterine function. J. Steroid Biochem. Mol. Biol. *102*, 41–50. https://doi.org/10.1016/j.jsbmb.2006.09.006.
52. Adams, N.R., and DeMayo, F.J. (2015). The Role of Steroid Hormone Receptors in the Establishment of Pregnancy in Rodents. Adv. Anat. Embryol. Cell Biol. *216*, 27–49. https://doi.org/10.1007/978-3-319-15856-3_3.
53. DeMayo, F.J., and Lydon, J.P. (2020). 90 YEARS OF PROGESTERONE: New insights into progesterone receptor signaling in the endometrium required for embryo implantation. J. Mol. Endocrinol. *65*, T1–T14. https://doi.org/10.1530/JME-19-0212.
54. Franco, H.L., Jeong, J.W., Tsai, S.Y., Lydon, J.P., and DeMayo, F.J. (2008). In vivo analysis of progesterone receptor action in the uterus during embryo implantation. Semin. Cell Dev. Biol. *19*, 178–186. https://doi.org/10.1016/j.semcdb.2007.12.001.
55. Simon, L., Spiewak, K.A., Ekman, G.C., Kim, J., Lydon, J.P., Bagchi, M.K., Bagchi, I.C., DeMayo, F.J., and Cooke, P.S. (2009). Stromal progesterone receptors mediate induction of Indian Hedgehog (IHH) in uterine epithelium and its downstream targets in uterine stroma. Endocrinology *150*, 3871–3876. https://doi.org/10.1210/en.2008-1691.
56. Large, M.J., and DeMayo, F.J. (2012). The regulation of embryo implantation and endometrial decidualization by progesterone receptor signaling. Mol. Cell. Endocrinol. *358*, 155–165. https://doi.org/10.1016/j.mce.2011.07.027.
57. Bhurke, A.S., Bagchi, I.C., and Bagchi, M.K. (2016). Progesterone-Regulated Endometrial Factors Controlling Implantation. Am. J. Reprod. Immunol. *75*, 237–245. https://doi.org/10.1111/aji.12473.
58. Wetendorf, M., Wu, S.P., Wang, X., Creighton, C.J., Wang, T., Lanz, R.B., Blok, L., Tsai, S.Y., Tsai, M.J., Lydon, J.P., and DeMayo, F.J. (2017). Decreased epithelial progesterone receptor A at the window of receptivity is required for preparation of the endometrium for embryo attachment. Biol. Reprod. *96*, 313–326. https://doi.org/10.1095/biolreprod.116.144410.
59. Roberson, E.C., Battenhouse, A.M., Garge, R.K., Tran, N.K., Marcotte, E.M., and Wallingford, J.B. (2021). Spatiotemporal transcriptional dynamics of the cycling mouse oviduct. Dev. Biol. *476*, 240–248. https://doi.org/10.1016/j.ydbio.2021.03.018.
60. Migone, F.F., Ren, Y., Cowan, R.G., Harman, R.M., Nikitin, A.Y., and Quirk, S.M. (2012). Dominant activation of the hedgehog signaling pathway alters development of the female reproductive tract. Genesis *50*, 28–40. https://doi.org/10.1002/dvg.20786.
61. Zacharias, W.J., Madison, B.B., Kretovich, K.E., Walton, K.D., Richards, N., Udager, A.M., Li, X., and Gumucio, D.L. (2011). Hedgehog signaling controls homeostasis of adult intestinal smooth muscle. Dev. Biol. *355*, 152–162. https://doi.org/10.1016/j.ydbio.2011.04.025.
62. Yang, Y., Paivinen, P., Xie, C., Krup, A.L., Makela, T.P., Mostov, K.E., and Reiter, J.F.

(2021). Ciliary Hedgehog signaling patterns the digestive system to generate mechanical forces driving elongation. Nat. Commun. *12*, 7186. https://doi.org/10.1038/s41467-021-27319-z.

63. Ramalho-Santos, M., Melton, D.A., and McMahon, A.P. (2000). Hedgehog signals regulate multiple aspects of gastrointestinal development. Development *127*, 2763–2772. https://doi.org/10.1242/dev.127.12.2763.
64. Huycke, T.R., Miller, B.M., Gill, H.K., Nerurkar, N.L., Sprinzak, D., Mahadevan, L., and Tabin, C.J. (2019). Genetic and Mechanical Regulation of Intestinal Smooth Muscle Development. Cell *179*, 90–105.e21. https://doi.org/10.1016/j.cell.2019.08.041.
65. Litingtung, Y., Lei, L., Westphal, H., and Chiang, C. (1998). Sonic hedgehog is essential to foregut development. Nat. Genet. *20*, 58–61. https://doi.org/10.1038/1717.
66. Pepicelli, C.V., Lewis, P.M., and McMahon, A.P. (1998). Sonic hedgehog regulates branching morphogenesis in the mammalian lung. Curr. Biol. *8*, 1083–1086. https://doi.org/10.1016/s0960-9822(98)70446-4.
67. Haraguchi, R., Yamada, G., Murashima, A., Matsumaru, D., Kitazawa, R., and Kitazawa, S. (2021). New Insights into Development of Female Reproductive Tract-Hedgehog-Signal Response in Wolffian Tissues Directly Contributes to Uterus Development. Int. J. Mol. Sci. *22*, 1211. https://doi.org/10.3390/ijms22031211.
68. Hsu, K.F., Pan, H.A., Hsu, Y.Y., Wu, C.M., Chung, W.J., and Huang, S.C. (2014). Enhanced myometrial autophagy in postpartum uterine involution. Taiwan. J. Obstet. Gynecol. *53*, 293–302. https://doi.org/10.1016/j.tjog.2013.01.030.
69. Wu, S.P., Wang, T., Yao, Z.C., Peavey, M.C., Li, X., Zhou, L., Larina, I.V., and DeMayo, F.J. (2022). Myometrial progesterone receptor determines a transcription program for uterine remodeling and contractions during pregnancy. PNAS Nexus *1*, pgac155. https://doi.org/10.1093/pnasnexus/pgac155.
70. Li, W.N., Dickson, M.J., DeMayo, F.J., and Wu, S.P. (2022). The role of progesterone receptor isoforms in the myometrium. J. Steroid Biochem. Mol. Biol. *224*, 106160. https://doi.org/10.1016/j.jsbmb.2022.106160.
71. Wu, S.P., and DeMayo, F.J. (2017). Progesterone Receptor Signaling in Uterine Myometrial Physiology and Preterm Birth. Curr. Top. Dev. Biol. *125*, 171–190. https://doi.org/10.1016/bs.ctdb.2017.03.001.
72. Oro, A.E., and Higgins, K. (2003). Hair cycle regulation of Hedgehog signal reception. Dev. Biol. *255*, 238–248. https://doi.org/10.1016/s0012-1606(02)00042-8.
73. Woo, W.M., Zhen, H.H., and Oro, A.E. (2012). Shh maintains dermal papilla identity and hair morphogenesis via a Noggin-Shh regulatory loop. Genes Dev. *26*, 1235–1246. https://doi.org/10.1101/gad.187401.112.
74. Li, C., Feng, C., Ma, G., Fu, S., Chen, M., Zhang, W., and Li, J. (2022). Time-course RNA-seq analysis reveals stage-specific and melatonin-triggered gene expression patterns during the hair follicle growth cycle in Capra hircus. BMC Genom. *23*, 140. https://doi.org/10.1186/s12864-022-08331-z.
75. Zhang, Y., Wu, K., Wang, L., Wang, Z., Han, W., Chen, D., Wei, Y., Su, R., Wang, R., Liu, Z., et al. (2020). Comparative study on seasonal hair follicle cycling by analysis of the transcriptomes from cashmere and milk goats. Genomics *112*, 332–345. https://doi.org/10.1016/j.ygeno.2019.02.013.
76. Marbach-Breitrück, E., Matz-Soja, M., Abraham, U., Schmidt-Heck, W., Sales, S., Rennert, C., Kern, M., Aleithe, S., Spormann, L., Thiel, C., et al. (2019). Tick-tock hedgehog-mutual crosstalk with liver circadian clock promotes liver steatosis. J. Hepatol. *70*, 1192–1202. https://doi.org/10.1016/j.jhep.2019.01.022.
77. Long, F., Zhang, X.M., Karp, S., Yang, Y., and McMahon, A.P. (2001). Genetic manipulation of hedgehog signaling in the endochondral skeleton reveals a direct role in the regulation of chondrocyte proliferation. Development *128*, 5099–5108. https://doi.org/10.1242/dev.128.24.5099.
78. Ajayi, A.F., and Akhigbe, R.E. (2020). Staging of the estrous cycle and induction of estrus in experimental rodents: an update. Fertil. Res. Pract. *6*, 5. https://doi.org/10.1186/s40738-020-00074-3.
79. Zeisel, A., Yitzhaky, A., Bossel Ben-Moshe, N., and Domany, E. (2013). An accessible database for mouse and human whole transcriptome qPCR primers. Bioinformatics *29*, 1355–1356. https://doi.org/10.1093/bioinformatics/btt145.
80. Kopinke, D., Roberson, E.C., and Reiter, J.F. (2017). Ciliary Hedgehog Signaling Restricts Injury-Induced Adipogenesis. Cell *170*, 340–351.e12. https://doi.org/10.1016/j.cell.2017.06.035.
81. Schmittgen, T.D., and Livak, K.J. (2008). Analyzing real-time PCR data by the comparative C(T) method. Nat. Protoc. *3*, 1101–1108. https://doi.org/10.1038/nprot.2008.73.
82. Lohman, B.K., Weber, J.N., and Bolnick, D.I. (2016). Evaluation of TagSeq, a reliable low-cost alternative for RNAseq. Mol. Ecol. Resour. *16*, 1315–1321. https://doi.org/10.1111/1755-0998.12529.
83. Meyer, E., Aglyamova, G.V., and Matz, M.V. (2011). Profiling gene expression responses of coral larvae (Acropora millepora) to elevated temperature and settlement inducers using a novel RNA-Seq procedure. Mol. Ecol. *20*, 3599–3616. https://doi.org/10.1111/j.1365-294X.2011.05205.x.
84. Ewels, P., Magnusson, M., Lundin, S., and Käller, M. (2016). MultiQC: summarize analysis results for multiple tools and samples in a single report. Bioinformatics *32*, 3047–3048. https://doi.org/10.1093/bioinformatics/btw354.
85. Bray, N.L., Pimentel, H., Melsted, P., and Pachter, L. (2016). Near-optimal probabilistic RNA-seq quantification. Nat. Biotechnol. *34*, 525–527. https://doi.org/10.1038/nbt.3519.
86. Gentleman, R.C., Carey, V.J., Bates, D.M., Bolstad, B., Dettling, M., Dudoit, S., Ellis, B., Gautier, L., Ge, Y., Gentry, J., et al. (2004). Bioconductor: open software development for computational biology and bioinformatics. Genome Biol. *5*, R80. https://doi.org/10.1186/gb-2004-5-10-r80.
87. Soneson, C., Love, M.I., and Robinson, M.D. (2015). Differential analyses for RNA-seq: transcript-level estimates improve gene-level inferences. F1000Res. *4*, 1521. https://doi.org/10.12688/f1000research.7563.2.
88. Love, M.I., Huber, W., and Anders, S. (2014). Moderated estimation of fold change and dispersion for RNA-seq data with DESeq2. Genome Biol. *15*, 550. https://doi.org/10.1186/s13059-014-0550-8.
89. Gu, Z., Eils, R., and Schlesner, M. (2016). Complex heatmaps reveal patterns and correlations in multidimensional genomic data. Bioinformatics *32*, 2847–2849. https://doi.org/10.1093/bioinformatics/btw313.

STAR★METHODS

KEY RESOURCES TABLE

REAGENT or RESOURCE	SOURCE	IDENTIFIER
Experimental models: Organisms/strains		
Progesterone receptor Cre mice	Jackson Labs	Stock: 017915; RRID: IMSR_JAX:017915
Smoothened floxed mice	Jackson Labs	Stock: 004526; RRID: IMSR_JAX:004526
Oligonucleotides		
See Table S1. Primers used for qPCR		
Other		
Masson Trichrome Stain kit	StatLab	Cat#: NC1052417
Hematoxylin and Eosin Stain kit	StatLab	Cat#: KTMTRLT
RNALater Storage Solution	Sigma	Cat#: R0901
QIAshredder column kit	Qiagen	Cat#: 79656
RNeasy mini kit	Qiagen	Cat#: 74106
iScript Reverse Transcription SuperMix	BioRad	Cat#: 1708841
MicroAmp Fast Optical 96 Well Reaction Plate	Thermofisher	Cat#: 43-469-06
SYBR Select Master Mix	Thermofisher	Cat#: 44-729-18

RESOURCE AVAILABILITY

Lead contact

Further information and requests for resources and reagents should be directed to and will be fulfilled by the lead contact, Elle Roberson (elle.roberson@cuanschutz.edu).

Materials availability

This study did not generate new unique reagents.

Data and code availability

3' TagSeq results have been deposited to NCBI GEO, under accession number GSE216120, and are publicly available as of the date of publication. This paper does not report original code. Any additional information required for reanalyze the data reported in this paper is available from the lead contact upon request.

EXPERIMENTAL MODEL AND STUDY PARTICIPANT DETAILS

Mice

6-8-week-old Swiss Webster female mice were obtained from Charles River, while *progesterone receptor cre* (*PR-Cre*, Stock: 017915)[32] and *smoothened* floxed (*Smo*$^{fl/+}$, Stock: 004526)[77] animals were obtained from Jackson Labs. Mice were group housed in individually ventilated cages in a pathogen-free facility with continuous food and water, with a controlled light cycle (light from 7am-7pm). Floxed females were bred to *PR-Cre*$^{+/-}$ males to produce experimental (*PR-Cre*$^{+/-}$; *Smo*$^{fl/fl}$, cKO) or littermate control females. 7-12-week-old females were estrous cycle staged using standard vaginal cytology[78] over the course of at least one month. Mice were humanely euthanized with extended CO_2 exposure followed by cervical dislocation, and female reproductive tracts were dissected. All animal experiments were approved by the University of Texas at Austin Institutional Animal Care and Use Committee.

METHOD DETAILS

Progesterone assay

Serum samples were collected by incubating mouse blood at room temperature for 60-90 minutes, then centrifuging at 2000 x g for 15min at room temperature. The serum was then removed and stored in a fresh microcentrifuge tube and stored at -20°C. Samples were sent to the University of Virginia Ligand Assay and Analysis Core for analysis in technical duplicate.

Tissue processing, histology, and immunofluorescence

Dissected uteri were gently affixed to a strip of index card to keep the tissue straight and fixed in 4% paraformaldehyde for either 4-6hr at room temperature (RT) or overnight at 4°C. Fixed uteri were washed in PBS, placed in 70% ethanol (EtOH) for at least 24hr, paraffin embedded, and transversely sectioned to produce 5μm sections. Sections were allowed to dry overnight.

For Hematoxylin and Eosin (H&E) staining, slides were baked at 60°C for 20min. Slides were de-waxed with three 5min xylene incubations, then rehydrated (100% EtOH, 3min x 2; 95% EtOH, 2min; and ddH2O, 4min). After rehydrating, slides were treated as follows: incubated in hematoxylin (3min), running tap water (1min), differentiated (45sec), water (30sec), bluing reagent (1min), water (30sec), 80% EtOH (1min), Eosin Y (3min), dehydrated (95% EtOH, 1min x 2; 100% EtOH, 3min x 2; xylene, 3min x 2), coverslipped with Cytoseal and allowed to cure overnight. H&E stained sections were imaged using a Keyence (BZ-X 710) or Leica DM6b microscope.

For Masson Trichrome staining, we used a Statlab kit (catalog #: KTMTRLT) and followed their instructions with some exceptions. In brief, slides were baked at 60°C for 20min, de-waxed in xylene (2x5min), and rinsed in 100% ethanol (3x1min) followed by running tap water (1min). Slides were then incubated in Bouin's Fluid (RT, overnight), rinsed in running tap water (3min), immersed in Hematoxylin (5min), rinsed in running tap water (2min), immersed in Biebrich Scarlet-Acid Fusion (1min), rinsed in running tap water (45min), immersed in Phosphomolybdic/ Phosphotungstic Acid (15min), then Aniline Blue stain (10min), rinsed in running tap water (1min), and then immersed in 1% Acetic Acid (5min). Finally, slides were dehydrated in 100% ethanol (3x1min), cleared with xylene (3x1min), and mounted with Cytoseal. Masson Trichrome stained slides were also imaged with the Keyence microscope.

RNA isolation and cDNA synthesis

For 3′ TagSeq (see below) of WT tissue, uterus samples were collected in triplicate at all estrous cycle stages. For qPCR, WT samples were collected (n=7) for each estrous cycle stage, and control and cKO samples (n=4) for estrus and diestrus. Following storage in RNA*Later* Storage Solution (Sigma, cat#: R0901) at -20°C, uterine tissue was physically lysed using a Beadbug 6 Microtube Homogenizer (Sigma-Aldrich, cat#: Z742682) and the lysate was spun through a QIAshredder column (Qiagen, cat#: 79656) to fully homogenize. A Qiagen RNeasy mini kit (Qiagen, cat#: 74106) was used to harvest RNA for RNAseq and qPCR. Total RNA was then either provided to the Genomic Sequencing and Analysis Facility at the University of Texas at Austin for 3′ TagSeq, or cDNA was synthesized using the iScript Reverse Transcription SuperMix (BioRad, cat#: 1708841) for qPCR.

qPCR

Most primers were designed from a database for mouse and human qPCR primers incorporated into the UCSC genome browser.[79] See Table S1 for primer details. We confirmed specificity of primers by ensuring that they BLAST to no more than 1 site in the genome and we only used primers whose melting curve displayed a single peak.

Primer sets were diluted from a stock (100μm in TE buffer) to 1μM in distilled deionized water. 2μL of each primer set (in technical quadruplicate) was allowed to dry in the bottom of a well in a MicroAmp Fast Optical 96 Well Reaction Plate (Thermofisher, cat#: 43-469-06). 10μL of a master mix of cDNA (250pg/well), SYBR Select Master Mix (Thermofisher, cat#: 44-729-18), and distilled deionized water was added to each well, the plates were sealed with MicroAmp Optical Adhesive Film (Thermofisher, cat#: 43-119-71) and allowed to incubate at RT in the dark for at least 15min to rehydrate primer. Plates were run on a ViiA-7 Real-Time PCR system (ThermoFisher), and CT values were auto-determined by the ViiA-7 software. The standard $2^{-\Delta\Delta Ct}$ method was then used to determine fold change based on the geomean of three 'housekeeping' genes (*Hprt*, *Dolk*, and *Sra1*).[80,81]

TagSeq

Tissue samples were collected in triplicate for each of the four estrous stages, accounting for 12 samples in total, and total RNA was collected as described above. Library preparation and sequencing for TagSeq,[82,83] a form of 3′ RNA sequencing, were performed by the Genomic Sequencing and Analysis Facility (GSAF) at The University of Texas at Austin. Total RNA was isolated from each sample by addition of Trizol (Thermo Fisher) and the sample was transferred to a Phasemaker tube (Thermo Fisher). Total RNA was extracted following the protocol supplied by the manufacturer and further cleaned up using a RNeasy MinElute Cleanup Kit (Qiagen). RNA integrity number (RIN) was measured using an Agilent Bioanalyzer and 100ng of RNA was used for the TagSeq protocol. The fragmentation/RT mix was prepared and added to each RNA sample, then heated to 95°C for 2.5 minutes on a Thermocycler and immediately put on ice for 2 minutes. After cooling and addition of the template switching oligo and SmartScribe RT, the fragmented RNA reaction was incubated at 42°C for 1hr, 65°C for 15 min. Next an AmPure bead clean-up was completed for the cDNA before it was amplified to incorporate the Illumina sequencing primer site, followed by another cleanup. The remaining portions of the Illumina adapter (the i5 and i7 indices) were then added through an additional 4 cycles of PCR. Final libraries were quantified with PicoGreen then pooled equally for size selection using the Blue Pippin from 355-550 bp. Resulting libraries were sequenced using an Illumina HiSeq 2500 instrument (50-nt single reads).

Sequence data pre-processing

Sequencing data quality was evaluated using the FastQC tool (v0.11.9)[48] and reports were aggregated with the MultiQC program (v1.0).[84]

QUANTIFICATION AND STATISTICAL ANALYSIS

Image quantitation

At least four sections over 100μm apart were imaged and quantified in order to accurately assess tissue morphology differences, and all quantitation was performed in FIJI. Keyence images were calibrated in FIJI based on the length of the scale bar. Uterine area was quantified in an unbiased manner by thresholding for uterine tissue and measuring the thresholded area. The lumen area was calculated by tracing along the apical edge of lumen epithelium. The stromal area was calculated by tracing along the stromal-myometrium junction and subtracting the lumen area. Uterine glands were counted with the multipoint tool, as previously described.[3] Longitudinal smooth muscle thickness was quantified by drawing a straight line from the outer edge of the circular muscle to the outer edge of the longitudinal muscle. Muscle fiber size and number was quantified using only Masson Trichrome staining, and the analysis started in Ilastik using the Pixel Classification mode.[41] First, we trained Ilastik on small images from each of our samples, classifying pixels as either muscle, collagen, or not-applicable. After training, Ilastik analyzed whole images to specify pixels and produce masks of the classification. Using FIJI we were able to focus specifically on the muscle mask and quantify both number and size using the Analyze Particles function. The statistical details of these experiments can be found in the figure legends.

TagSeq data analysis

Single-end pseudo-alignment was performed against the mouse transcriptome (GENCODE M25 transcript sequences) using kallisto (v0.45.0)[85] with options -l 200 -s 50 –single-overhang –bias. Downstream analysis of transcript abundance data was performed in R following protocols outlined in Bioconductor.[86] The tximport package[87] was used to roll up transcript-level counts into gene-level counts provided to the DESeq2 package.[88] Count data matrices were filtered to remove genes with fewer than 1 read across all included samples. We used estrous stage as the model to explore gene expression changes across the cycle, where the samples were pooled based on cycle stage. Differentially expressed gene (DEGs) results reported are those with maximum adjusted p-value 0.05 and log2 fold change greater than 1.0 or less than -1.0. Heatmaps were made using z-scores based on the VSD and ComplexHeatmap[89] in R. Volcano plots were made according to the DESeq2 vignette. The statistical details of these experiments can be found in the figure legends.